DEVELOPMENT OF SEMI-AUTOMATIC LIVER SEGMENTATION METHOD FOR THREE-DIMENSIONAL COMPUTED TOMOGRAPHY DATASET

CHIANG YI FAN

UNIVERSITI SAINS MALAYSIA

2017

DEVELOPMENT OF SEMI-AUTOMATIC LIVER SEGMENTATION METHOD FOR THREE-DIMENSIONAL COMPUTED TOMOGRAPHY DATASET

by

CHIANG YI FAN

Thesis submitted in partial fulfilment of the
requirements for the degree of
Bachelor of Engineering (Electronic Engineering)

JUNE 2017

ACKNOWLEDGEMENT

TABLE OF CONTENTS

LIST OF TABLES

LIST OF FIGURES

LIST OF ABBREVIATIONS

3D	Three Dimensional
3DIRCADb	3D Image Reconstruction for Comparison of Algorithm Database
ASD	Average Symmetric Surface Distance
CT	Computed Tomography
GLOBOCAN	Global Cancer Incidence, Mortality, and Prevalence
GUI	Graphical User Interface
GVF	Gradient Vector Flow
MICCAI	Medical Image Computing and Computer-Assisted Intervention
MRI	Magnetic Resonance Imaging
MSD	Maximum Symmetric Surface Distance
OpenCV	Open Source Computer Vision
RF	Radio Frequency
RMSD	Root Mean Square Symmetric Surface Distance
RVD	Relative Volume Difference
SLIVER07	Segmentation of the Liver Competition 2007
VOE	Volumetric Overlap Error
WHO	World Health Organization

PEMBANGUNAN KAEDAH PERUASAN HATI SEPARA-AUTOMATIK DARIPADA DATASET TOMOGRAFI BERKOMPUTER TIGA DIMENSI

ABSTRAK

Peruasan hati daripada dataset tiga dimensi tomografi berkomputer (CT) adalah sangat penting dalam diagnosis dan perancangan rawatan penyakit hati. Peruasan manual memberi keputusan yang lebih tepat tetapi meletihkan dan memakan masa kerana kepingan imej yang banyak dihasilkan oleh mesin CT. Beza jelas yang rendah pada sempadan hati dengan organ-organ berjiranan, kepelbagaian yang tinggi bentuk-bentuk hati dan kehadiran pathologi hati akan menjejaskan ketepatan peruasan hati automatik dan menjadikan peruasan hati automatic satu tugas yang mencabar. Oleh itu, perisian peruasan separa-automatik telah dibina dalam projek ini untuk memperoleh ketepatan peruasan hati yang tinggi dan mengurangkan masa yang digunakan untuk peruasan hati secara manual. Algoritma yang dicadangkan boleh dibahagikan kepada tiga peringkat. Peringkat pertama ialah persiapan parameter dan pra-pemprosesan. Dalam pra-prosesan, keadah resapan tak-isotropi digunakan untuk mengurangkan hingar dalam imej dan melicinkan imej. Dalam peringkat kedua, teknik pengambangan digunakan untuk mendapatkan kawasan hati dalam imej CT. Selepas itu, mophologi penutupan dan pembukaan digunakan untuk menutup lubang-lubang kecil dalam kawasan hati dan memutuskan sambungan nipis di antara hati dengan organ-organ berjiranan. Kemudian, penutupan lubang digunakan untuk mengisi lubang-lubang besar dalam kawasan hati. Selepas itu, analisis komponen-komponen bersambung akan dijalankan untuk menyarikan kawasan hati daripada kepingan imej CT. Peringkat terakhir merupakan pasca-pemprosesan. Dalam pasca-pemprosesan, kontur hati dilicinkan dengan turas Gauss perduaan. Perisian peruasan hati dengan algoritma yang dicadangkan dinilai dengan menggunakan dataset CT yang diperoleh daripada SLIVER07 untuk membuktikan keberkesanannya dalam peruasan hati. Keputusan peruasan hati mencapai purata VOE 9.93 ± 4.36 %, purata RVD -0.03 ± 3.76 %, purata ASD 2.57 ± 1.73 mm, purata RMSD 5.82 ± 3.56 mm dan purata MSD 39.90 ± 17.23 mm. Jumlah masa yang diperlukan oleh perisian yang dibina untuk menyelesaikan proses peruasan hati adalah di antara 2 hingga 4 minit. Algoritma yang dicadangkan dapat meruas hati yang sihat dengan cekap dan berkesan walaupun terdapat masalah peruasan berlebihan dan masalah peruasan berkurangan disebabkan kehadiran penyakit dan beza jelas yang rendah di antara hati dengan organ-organ berjiranan.

DEVELOPMENT OF SEMI-AUTOMATIC LIVER SEGMENTATION METHOD FOR THREE DIMENSIONAL COMPUTED TOMOGRAPHY DATASET

ABSTRACT

Segmentation of liver from 3D computed tomography (CT) dataset is very important in hepatic disease diagnosis and treatment planning. Manual segmentation gives accurate result but the process is tedious and time-consuming due to a large number of slices produced by the CT scanner. Low contrast of liver boundary with neighbouring organs, high shape variability of liver and presence of various liver pathologies will affect the accuracy of automatic liver segmentation and thus make automatic liver segmentation a challenging task. Therefore, a semi-automated liver segmentation program is developed in this project in order to obtain high accuracy in liver segmentation and reduce the time required for manual liver segmentation. The proposed algorithm can be divided into three stages. The first stage is parameter setup and pre-processing. User interaction is required to setup the segmentation parameters. For pre-processing, anisotropic diffusion filtering is applied to reduce noise in the image and smooth the image. In second stage, thresholding is applied to CT images to extract the possible liver regions. Then, morphological closing and opening are used close small holes inside liver region and break the thin connections between liver and neighbouring organs. Hole-filling is employed to fill up the large holes inside liver region. Next, the connected component analysis is performed to extract liver region from the CT slices. The last stage is post-processing. In post-processing, the contour of liver is smooth by binary Gaussian filter. The liver segmentation program with proposed algorithm is evaluated with CT datasets obtained from SLIVER07 to prove its effectiveness in liver segmentation. The results of liver segmentation achieved average VOE of 9.93 ± 4.36 %, average RVD of -0.03 ± 3.76 %, average ASD of 2.57 ± 1.73 mm, average RMSD of 5.82 ± 3.56 mm, and average MSD of 39.90 ± 17.23 mm. The total time required for the program developed to complete liver segmentation process is between 2 to 4 minutes. The proposed algorithm was able to segment the healthy liver effectively and efficiently even though there were over-segmentation and under-segmentation problem due to the presence of pathologies and low contrast between liver and neighbouring organs.

CHAPTER ONE
INTRODUCTION

1.1   Background

Liver is the largest glandular organ in our body. It is located at the upper-right section of abdominal cavity to the right of stomach as shown in Figure 1.1. The liver plays important roles in keeping the body pure from toxins and harmful substances. Among the functions of liver are haemoglobin decomposition, protein synthesis, glycogen storage, storage of vitamins and minerals, detoxification, hormone regulation and bile production (Jayanthi, 2016; Starr & McMillan, 2016).
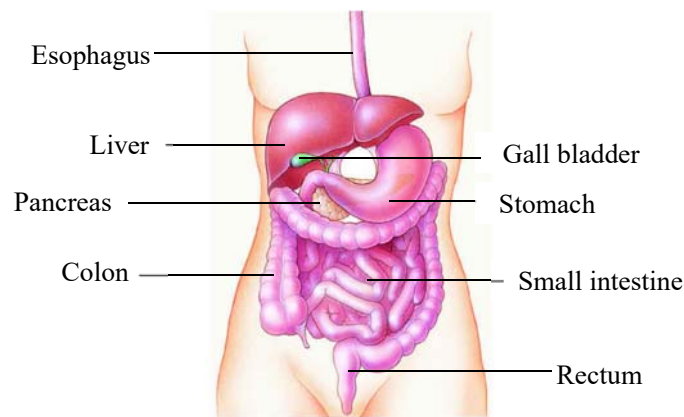
Figure 1.1: Location of liver in human abdominal cavity (Starr & McMillan, 2016)

Liver is prone to many diseases such as hepatitis A, hepatitis B, hepatitis C, cirrhosis and liver cancer (Younossi *et al.*, 2011). According to Global Cancer Incidence, Mortality and Prevalence (GLOBOCAN), which is an international agency for research on cancer under World Health Organization (WHO), liver cancer has become the second common causes of cancer death (Ferlay *et al.*, 2013). Liver cancer caused 745,000 deaths worldwide in 2012 (Ferlay *et al.*, 2015). In Malaysia, liver cancer caused 1,600 death in 2010 and the figure was increased to 1,900 death in 2015 (WHO, 2016).

Computer aided liver diagnosis plays an important role in helping doctors to diagnose liver diseases and plan proper treatment (Luo *et al.*, 2014). Diagnosis of liver diseases can be done by using medical imaging modalities such as ultrasonography, computed tomography (CT) and magnetic resonance imaging (MRI). Ultrasonography is safe because it uses high frequency sound wave instead of ionising radiation but its accuracy is lower than CT and MRI. CT scan uses X-ray and provides high accuracy images. MRI uses strong magnetic field and high radiation

radio waves to get detailed image (Jayanthi, 2016). Among these imaging modalities, CT is commonly used because it is well-established for non-invasive diagnosis of liver diseases due to advanced technology in CT scanner and image reconstruction algorithm (Li *et al.*, 2015).

Liver segmentation is a process to divide a medical image obtained from imaging modalities such as computed tomography (CT) and magnetic resonance imaging (MRI) into liver parenchyma area and non-liver parenchyma area (Luo *et al.*, 2014). Liver segmentation is important in computer aided liver diagnosis to evaluate patient-specific liver anatomy for hepatic disease diagnosis, function assessment, and treatment planning (Li *et al.*, 2015). Traditionally, doctors or radiologists segment liver region manually. Yet, manual segmentation is difficult, time-consuming and doctors or radiologists need to have experience in the liver segmentation to obtain accurate results. Hence, it is a goal to segment liver region fast and accurately (Lu *et al.*, 2014).

Semi-automatic or automatic liver segmentation is preferable and helpful in clinical application (Li *et al.*, 2015). Many methods have been proposed to segment liver effectively and efficiently. The methods used in semi-automatic and automatic liver segmentation include threshold based, region growing, active contour, graph cuts, and clustering based (Luo *et al.*, 2014). Liver segmentation is a challenging task in medical image processing due to high shape variability of liver, low contrast with adjacent organs or tissues and presence of various pathologies such as tumours. Besides, image artefacts and noise presence may lead to blurred boundaries between liver and neighbouring organs and affect the accuracy of segmentation (Li *et al.*, 2015; Peng *et al.*, 2015).

1.2   Problem Statements

One challenge in automatic liver segmentation is the accuracy of segmentation. In automatic liver segmentation, low contrast of liver boundary with adjacent organs may lead to over-segmentation problem in grey-level based methods (Irr & Rahni, 2015). The artefacts and noise presence in CT image that blurred the liver boundary will affect the liver segmentation accuracy for pixel-based approaches such as thresholding, region growing, and edge detection because these methods are very sensitive to noise (Li *et al.*, 2015). The presence of large tumours and other liver pathologies leads to inhomogeneous appearance in CT images which may cause misclassification of the tumours as non-liver tissue in region growing and clustering-based methods (Peng *et al.*, 2015).

Segmentation of liver manually by radiologists is a tedious and time-consuming task due to large number of CT slices produced by high resolution CT scanner. The difficulty of manual liver segmentation increases due to the complexity and variability of liver shape (Arjun *et al.*, 2015). The time required for a radiologist to segment liver from a CT dataset with 320 slices is about 4 hours. The manual segmentation results are greatly depend on the skill of the radiologist or doctor so human error may affect the segmentation results (Goryawala *et al.*, 2012).

Parameter configuration is time-consuming too. This is because there are more than one parameter to be configured in image processing operations such as image filtering and morphological image processing. It is better to find out the optimum values for the parameters experimentally and set the optimum values as default values of the parameters in term of performance consideration (Li *et al.*, 2015).

1.3   Project Objectives

The objectives of this project are:
1. To develop a semi-automatic liver segmentation program.
2. To determine the optimum values for parameters of image filtering and morphological operations.
3. To evaluate the performance of the developed program in term of segmentation accuracy and segmentation time.

1.4   Scope of Project

The scope of project is to develop a semi-automatic program for liver segmentation. The program developed is written by using C++ programming language with Open Source Computer Vision (OpenCV) library. Graphical user interface (GUI) is created to aid user to use the program easily.

In this project, only abdominal CT images will be dealt with. The 3D abdominal CT datasets are obtained from Segmentation of the Liver Competition 2007 (SLIVER07) website, http://www.sliver07.org/download.php. Each datasets consists of 64 to 394 CT slices (Heimann *et al.*, 2009).

1.5 Chapter Organization

This report consists of five chapters. Chapter 1 gives an introduction to the project which includes the background of the project, problem statement, objectives, and scope of project.

Chapter 2 contains the literature review which describes the previous techniques developed for liver segmentation. This chapter explains the imaging modalities used in abdominal image acquisition. Various approaches used in liver segmentation are explained in this chapter.

Chapter 3 presents methodology of this project. In this chapter, the concepts and algorithm used in liver segmentation are discussed and explained in detail. The design of graphical user interface and the program workflow are described in this chapter.

Chapter 4 explains the CT dataset used for evaluation. The optimisation processes of anisotropic diffusion filtering and morphological operation are explained in detail. The evaluation methods of the segmentation result are presented in this chapter. The evaluation results obtained are analysed and discussed in detail. The quantitative comparison of proposed method with methods developed by other researchers is presented in this chapter.

Chapter 5 presents the conclusion of this final year project. Some recommendations on future improvements are expressed in this chapter.

CHAPTER TWO
LITERATURE REVIEW

2.1   Introduction

As mentioned in Chapter 1, diagnostic imaging modalities such as ultrasonography, computed tomography (CT) and magnetic resonance imaging (MRI) can be used to obtained abdominal images for diagnosis of liver diseases. The working principles of modalities used to obtained abdominal images are discussed in section 2.2.

Image segmentation is a process of decomposition of image into multiple parts for analysis. The analysis usually involves object identification or attribute extraction of digital image. The level of detail of decomposition process depends on the object to be identified or attribute to be extracted. Once the object is identified or attribute is extracted, the segmentation process will be stopped. To improve the accuracy of segmentation, considerable care should be taken especially when dealing with segmentation of nontrivial images (Gonzalez & Woods, 2006). The methods used in pre-processing of abdominal images to improve the segmentation result are presented in section 2.3. The common techniques used in liver segmentation are discussed in section 2.4.

2.2   Modalities in Diagnostic Imaging

Different modalities are used by radiologist and doctor to view the internal parts of body. The common imaging modalities used in early diagnosis of liver diseases are ultrasonography, computed tomography (CT) and magnetic resonance imaging (MRI) (Jayanthi, 2016). The working principles of ultrasonography, computed tomography (CT) and magnetic resonance imaging (MRI) are discussed in the subsections below.

2.2.1   Ultrasonography

In ultrasonography, ultrasonography machine as shown in Figure 2.1(a) is used to acquire image. Gel that acts as acoustic seal is applied on the patient's skin and transducer as shown in Figure 2.1(b) that emits and receives high frequency sound waves is moved across the surface of patient's body. The image is generated by scan converter at real time based on the intensity of returning echo and the duration for the sound wave to reflect back to the transducer. The intensity of returning echo of tissues such as abdominal fats that have higher echogenicity than other soft tissues will appear brighter on ultrasound image. These tissues are described as hyperechoic. Tissues that have lower intensity of returning echo will appear darker on ultrasound images and

are known as hypoechoic. Fluid-filled structures such as gall bladder and urinary bladder appear as black due to few or no acoustic interfaces (Eastman *et al.*, 2006; Singh & Neutze, 2015).

(a)   (b)
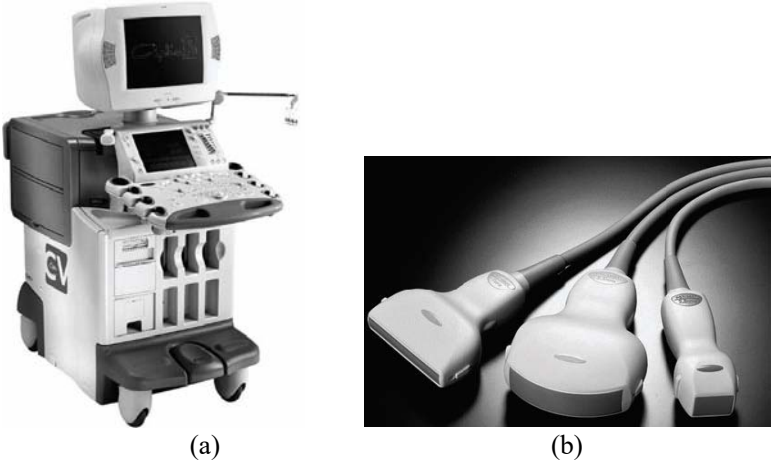
Figure 2.1: (a) Ultrasonography machine, (b) Transducers for different purpose (Eastman *et al.*, 2006)

The image is often recorded with 512 × 512 or 640 × 480 pixels with bit depth of 8 bits for grey image. For colour image, bit depth of 24 bits is used, one byte each for red, green and blue channels. For video clip acquisition, the video is taken at 10 to 30 frames per seconds (Bushberg *et al.*, 2012). Figure 2.2 shows ultrasonography (USG) image of abdomen which shows that there a solid echogenic mass (M) between liver and right kidney (RK) (Bano *et al.*, 2012).
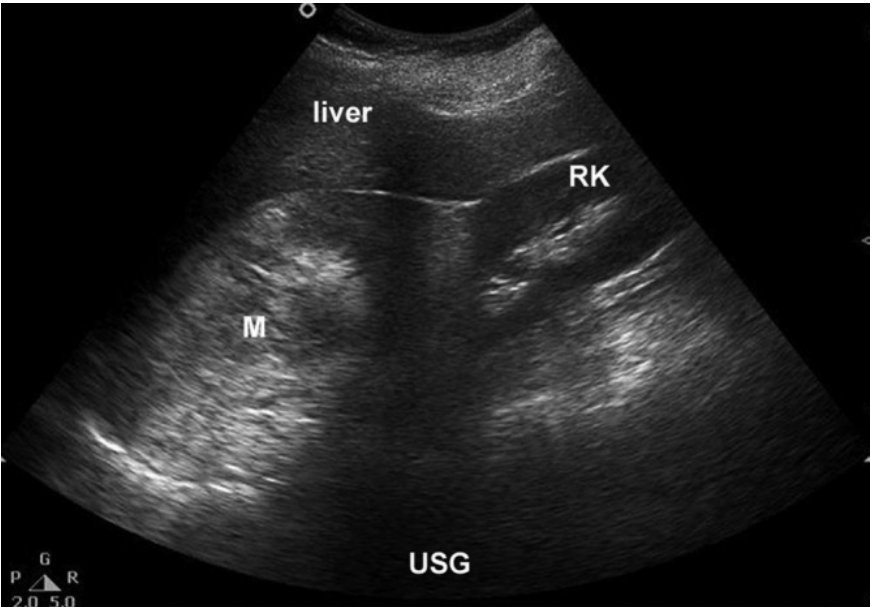
Figure 2.2: Ultrasound image of abdomen (Bano *et al.*, 2012)

2.2.2 Computed Tomography (CT)

In computed tomography (CT), the images are acquired by measuring the X-ray transmission profiles through a patient from different angle around the body. Figure 2.3 shows anatomical planes of body. From the figure, the axial plane divides the body into upper and lower segments, the coronal plane divides the body into front and back sections, and the sagittal plane divides body into left and right sections. Figure 2.4 shows a patient is placed in CT gantry and CT image acquisition in axial sections. During CT scanning, the X-ray tube rotates continuously around patient. A beam of X-ray passes through patient's body and hits detector arc which consists of row of detector elements. Rapid acquisition can be achieved by using multiple detector rows. When the X-ray beam passes through patient's body, the tissues with different density will have different linear attenuation coefficients to the X-ray beam. The detector samples and digitises the incoming radiation signal and send to computer for image reconstruction (Dance *et al.*, 2014; Smith & Farrell, 2014; Singh & Neutze, 2015).
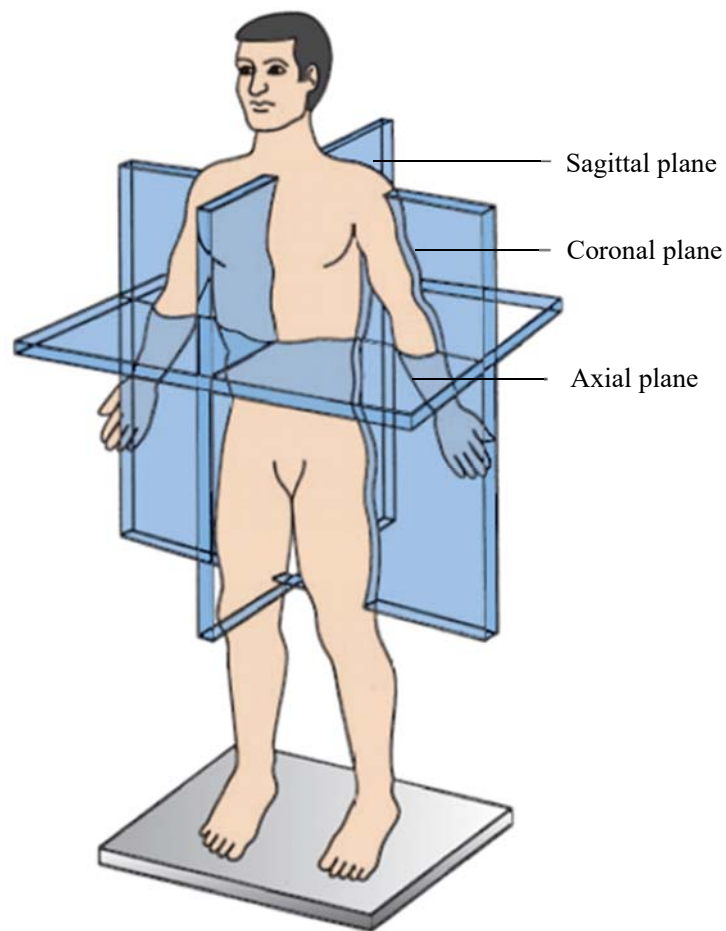
Figure 2.3: Anatomical planes of body (Smith & Farrell, 2014)

Figure 2.4: A patient is placed in CT gantry and CT image acquisition in axial sections (Singh & Neutze, 2015)

Image reconstruction algorithm is applied to restructure the raw data. The average linear attenuation coefficient for each projection of a pixel is computed and stored in a 3D matrix of pixels. The value of pixel represents the linear attenuation coefficients and is expressed as Hounsfield units (HU). Hounsfield units range from -1000 for air to 1000 for dense bone and water is represented as zero. For clinical imaging, minimum bit depth used for Hounsfield scale should be 12, so that it can cover most clinical relevant tissues. Hounsfield scale can be extended to bit depth of 14 to make it compatible with high linear attenuation coefficient materials. CT images usually store as raw or DICOM format with bit depth of 16 bits (Dance *et al.*, 2014; Washington & Leaver, 2015). Figure 2.5 shows an abdominal axial CT image with dense bone appears as white and soft tissue appears as grey (Bano *et al.*, 2012).
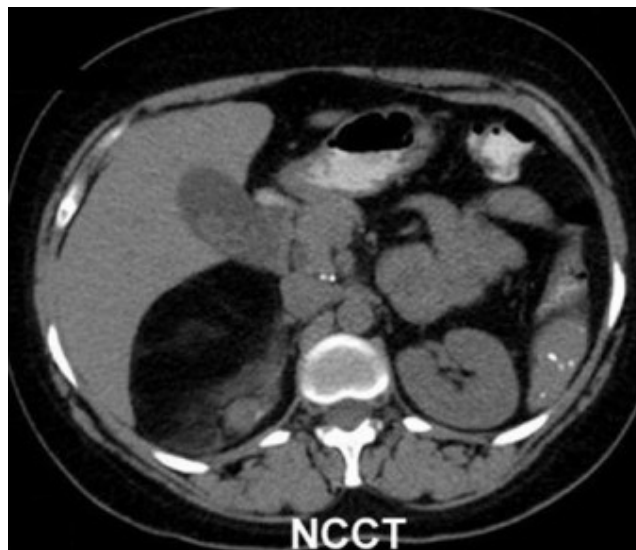
Figure 2.5: Abdominal axial CT image (Bano *et al.*, 2012)

2.2.3 Magnetic Resonance Imaging (MRI)

Magnetic resonance is based on the interaction between applied magnetic field and angular momentum of nuclear spin. In magnetic resonance imaging (MRI), the patient is exposed to strong magnetic field and radio frequency (RF) wave in MRI scanner as shown in Figure 2.6. In MRI, RF pulse which has the same frequency as the spin frequency of hydrogen nuclei is applied to the patient. The hydrogen nuclei become energised or resonate after absorbed the RF pulse energy. Once the RF pulse is stopped, the excited hydrogen nuclei immediately decay back to their steady state by emitting RF signal. This process is known as relaxation. The intensity of RF signal emitted which represents the number of hydrogen nuclei and location is captured by the receiver coil. If high number of hydrogen atoms present, for example in fat, the received RF signal will be intense whereas if the low number of hydrogen atoms present, for example in bone, the received RF signal will have low intensity (Eastman *et al.*, 2006; Singh & Neutze, 2015).

Figure 2.6: MRI scanner (Eastman *et al.*, 2006)

The MRI scanner can measure relaxation times, T1 and T2. The T1 relaxation time is also known as longitudinal relaxation time or spin-lattice relaxation time, is the time required for the excited hydrogen nuclei to return to their original orientation in the direction of applied magnetic field by giving up their energy. One T1 is equal to time required to return to 63% of its original value once the RF excitation pulse stopped. T2 relaxation time is also known as spin-spin relaxation time or transverse relaxation time, is the time required for the transverse magnetisation components of the excited hydrogen nuclei to decay to 37% of its initial value immediately after 90º RF pulse when irreversible loss of phase coherence to the spin occurs. T2* is another source that contributes to the total relaxation time. T2* relaxation is an exponential decay of transverse magnetisation M_{XY} immediately after the excitation pulse as a function with time constant T2*. T2* relaxation time depends on the main field inhomogeneity and magnetic susceptibility (McRobbie *et al.*, 2006).

MRI images usually stored in raw or DICOM format with depth of 16-bit. There are two common sequences in MRI known as T1-weighted and T2-weighted sequences. In T1-weighted image, fluids are very dark, water-based tissues are mid-grey and fat-based tissues are very bright, with different soft tissues have intensity in between. In T2-weighted image, water is bright and fat is dark, with different soft tissues have intensity in between (McRobbie *et al.*, 2006). Figure 2.7 shows example of T1-weighted and T2-weighted abdominal images (Bano *et al.*, 2012).

(a)	(b)
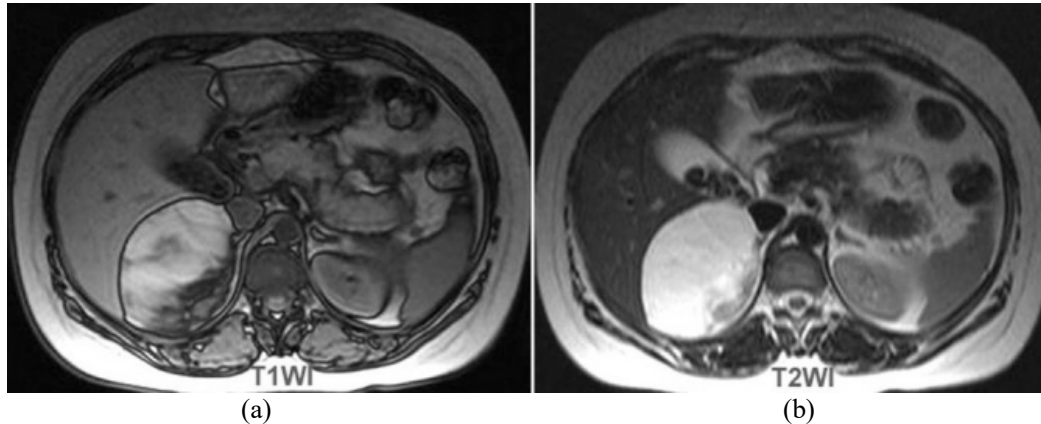
Figure 2.7: (a) T1-weighted abdominal axial image, (b) T2-weighted abdominal axial image (Bano *et al.*, 2012)

2.2.4 Comparison of Diagnostic Imaging Modalities

Ultrasonography is safe as it does not require the use of ionising radiation. Ultrasonography is relatively cheaper than other imaging modalities like CT and MRI. In addition, it is fast and can produce slices in multiple planes at real time. Besides, portable unit is available to be used in emergency situations. However, ultrasonography is not good for bone and lung imaging and the detection of malignant lump required skilled operator (Smith & Farrell, 2014).

One advantage of MRI is it does not use ionising radiation as in CT. During CT scan, patient is exposed to radiation of X-rays beam, so it is not recommended for pregnant women and children. CT is good for axial imaging whereas MRI is good for coronal and sagittal imaging. CT has higher spatial resolution than MRI but soft tissue contrast of MRI is better than soft tissue contrast of CT (Smith & Farrell, 2014). MRI is generally more costly than CT and the image acquisition time is longer as compared to CT. MRI is not able to scan patients with ferromagnetic material in their body (Singh & Neutze, 2015). Long scan time of MRI may result in motion artefacts in the images acquired. Single breath-hold is required for abdominal CT scan to prevent motion artefacts (Smith & Farrell, 2014). The advantages and disadvantages of the three modalities are summarised in Table 2.1.

Table 2.1: Comparison of diagnostic imaging modalities (Smith & Farrell, 2014; Singh & Neutze, 2015)

	Ultrasonography	CT	MRI
Technology used	Ultrasound wave	X-ray	Magnetic field and RF wave
Advantages	- Safe, no ionising radiation - Less expensive than CT and MRI - Multiple plane imaging - Real-time imaging - Portable	- Good for axial imaging - Scans are performed faster than MRI - Higher spatial resolution than MRI	- Good for coronal and sagittal imaging - Soft tissue contrast is better than CT - No ionising radiation
Disadvantages	- Not good for bone and lung imaging - Required skilled operator to detect malignant lump	- Expensive - Patient is exposed to radiation of X-rays beam, not recommended for pregnant women and children - Single breath-hold is required to prevent motion artefacts	- More expensive than CT - Takes longer time to scan than CT - Inability to scan patient with ferromagnetic material in the body. - Motion artefacts due to long scan time

2.3 Image Pre-Processing

Image pre-processing is an important step to reduce noise and smooth the images. Lu *et al.* (2014) applied Gaussian filter to smooth the image and reduce noise effects so that the complexity of segmentation process can be reduced. Li *et al.* (2013) improved segmentation result of fuzzy clustering by employing median filter to reduce noise and smooth the image. Suzuki *et al.* (2010) applied anisotropic diffusion as pre-processing step to improve the accuracy of geodesic active contour. Anisotropic diffusion is capable of reducing noise and preserving the structure of liver.

Noise reduction improves overall accuracy of liver segmentation. Salt and pepper noise in CT images that reduces the accuracy of liver segmentation can be reduced by smoothing filter (Priyadarsini & Selvathi, 2012). Smoothing filters are applied to blur and suppress noise of an image. The filters can be classified into linear and non-linear filter. For linear filters, there is one-to-one relationship between spatial and frequency domains. Gaussian filter is an example of linear filter whereas median filter and anisotropic diffusion are examples of non-linear filter (Gonzalez & Woods, 2006). The common filters used in pre-processing stage are explained in following subsections.

2.3.1 Gaussian Filter

Gaussian filter is a lowpass filter that replace a pixel with weighted average of the neighbouring pixels. Gaussian filter is used in noise suppression because it can reduce sharp intensity transitions. However, it introduces blurring effects to the edges as sharp intensity transitions occur at edges. Figure 2.8(a) shows a 3×3 average smoothing filter mask. Gaussian filter as shown in Figure 2.8(b) is formed by introducing weightage to the average filter mask. The rest of the pixels are weighted using Gaussian distribution function (Gonzalez & Woods, 2006).

$$\frac{1}{9} \times \begin{array}{|c|c|c|} \hline 1 & 1 & 1 \\ \hline 1 & 1 & 1 \\ \hline 1 & 1 & 1 \\ \hline \end{array} \qquad \frac{1}{16} \times \begin{array}{|c|c|c|} \hline 1 & 2 & 1 \\ \hline 2 & 4 & 2 \\ \hline 1 & 2 & 1 \\ \hline \end{array}$$

(a)   (b)
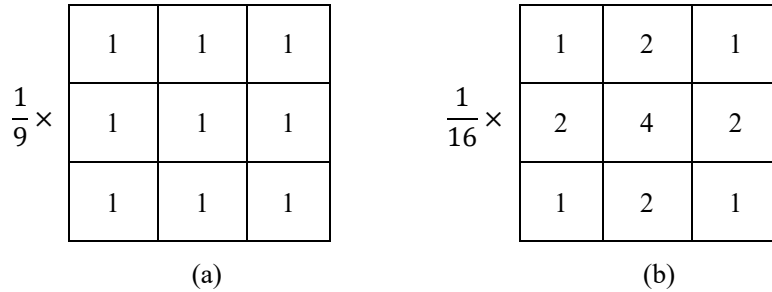
Figure 2.8: (a) 3×3 average filter mask, (b) 3×3 Gaussian filter mask (Gonzalez & Woods, 2006)

The 2D Gaussian distribution function, $G(x, y)$ is given by Eq. (3.4) (Sonka *et al.*, 2008).

$$G(x, y) = e^{-\frac{x^2 + y^2}{2\sigma^2}} \tag{2.1}$$

where x and y are spatial coordinates of image and σ is the standard deviation of the probability distribution. The standard deviation σ is proportional to the size of neighbouring pixels on which the filter operates. The pixel at the centre of mask is more important, thus it is assigned with higher value than the neighbouring pixels. The pixels which are further away from the centre of the mask have smaller influence, thus the values assigned are smaller (Gonzalez & Woods, 2006; Sonka *et al.*, 2008).

2.3.2 Median Filter

Median filter is a non-linear filter that provides excellent noise reduction capability and reduces the blurring effect of the edges as in Gaussian filter. Median filter replaces each pixel value by the median pixel value in a square neighbourhood around the centre pixel. For example, in 3×3 median filter, the values of pixel in 3×3 neighbourhood will be sorted and the fifth largest value will be assigned to the corresponding pixel as shown in Figure 2.9(a). The asterisks as shown in Figure 2.9(b) represent values of pixel that remain the same after filter is applied (Gonzalez & Woods, 2006).

70	84	96
84	70	80
88	79	75

*	*	*
*	80	*
*	*	*

(a)   (b)

Figure 2.9: (a) Pixel values before median filter is applied, (b) Pixel values after median filter is applied (Gonzalez & Woods, 2006)

Median filter is effective in impulse noise reduction. However, median filter could damage the thin line or sharp corner in the image. This is because the principle function of median filter is to force points with distinct intensity to be similar to their neighbourhood. Hence, small isolated cluster of pixels that are lighter or darker with respect to their neighbouring pixels and whose area is smaller than one-half of the filter area are eliminated by median filter (Gonzalez & Woods, 2006; Sonka *et al.*, 2008).

2.3.3 Anisotropic Diffusion

Anisotropic diffusion is often used as pre-processing step to filter noise and preserves edges or other important details. Anisotropic diffusion is modelled as a diffusion that is allowed along homogeneous regions and inhibited by region boundaries (Yussof & Burkhardt, 2009). The drawback of anisotropic diffusion filtering is it requires more computational time due to the iterative diffusion process (Priyadarsini & Selvathi, 2012).

Anisotropic diffusion equation was formulated by Perona and Malik (1990). The equation is based on the numerical solution of non-linear partial differential equation on two-dimensional image. The partial differential equation used to describe the diffusion process is given by Eq. (2.2) (Perona & Malik, 1990)

$$\frac{\partial I}{\partial t} = \text{div}(c(x, y, t)\nabla I) = c(x, y, t)\Delta I + \nabla c \cdot \nabla I \tag{2.2}$$

where div is divergence operator, ∇ is gradient operator with respect to space variables, Δ is Laplacian operator with respect to the space variables, I is the input image and c is the proposed flux function which controls the rate of diffusion at any point in the image. Two flux functions as shown in Eq. (2.3) and Eq. (2.4) were proposed (Perona & Malik, 1990).

$$c(\|\nabla I\|) = e^{-\left(\frac{\|\nabla I\|}{K}\right)^2} \tag{2.3}$$

$$c(\|\nabla I\|) = \frac{1}{1 + \left(\frac{\|\nabla I\|}{K}\right)^2} \tag{2.4}$$

The constant K is used to control the filter sensitivity to edge contrast and is either chosen manually or as function of noise in the image. Eq. (2.3) and Eq. (2.4) are different as Eq. (2.3) privileges high contrast edge over low contrast one whereas Eq. (2.4) privileges wide region over small region (Perona & Malik, 1990).

The Eq. (2.2) can be discretized by using 4-nearest-neighbours discretization of Laplacian operator. The discretized equation is given by Eq. (2.5) (Perona & Malik, 1990).

$$I_{i,j}^{t+1} = I_{i,j}^t + \lambda \left[c_N \cdot \delta_N I + c_S \cdot \delta_S I + c_E \cdot \delta_E I + c_E \cdot \delta_E I\right]_{i,j}^t \tag{2.5}$$

The subscripts $N, S, E,$ and W correspond to pixels on the above (North), on the below (South), on the right (East) and on the left (West) of the pixel under consideration at coordinate (i, j). The symbol δ is nearest neighbour differences, t is number of iterations and λ is stability factor that in the range of 0 to 0.25 for the numerical scheme to be stable (Perona & Malik, 1990).

2.4   Image Segmentation Techniques

In diagnostic radiology, liver segmentation is important in diagnosis of liver pathologies. Various methods used for liver segmentation are based on threshold, region growing, active contour, graph cuts and clustering. Some of the methods are semi-automatic which need user to select the region of interest before computer processing. Fully automated segmentation methods segment the images without user intervention (Priyadarsini & Selvathi, 2012). The various approaches used in liver segmentation are discussed in subsections below.

2.4.1   Thresholding

Thresholding is the simplest segmentation method and useful if the region of interest has good contrast with other regions in the image. If the pixel intensity, $f(x, y)$ falls between lower threshold, T_1 and upper threshold, T_2, the output pixel $g(x, y)$ will be assigned to white whereas if the pixel intensity, $f(x, y)$ falls outside the threshold range, the output pixel, $g(x, y)$ will assigned to be black as shown in Eq. (2.6) (Dance *et al.*, 2014).

$$g(x, y) = \begin{cases} 1 & T_1 \leq f(x, y) \leq T_2 \\ 0 & otherwise \end{cases} \tag{2.6}$$

Another approach is if the pixel intensity, $f(x, y)$ falls between lower threshold, T_1 and upper threshold, T_2, the pixel intensity will be maintained whereas pixels with intensity which is out of the threshold range will assigned to be black as shown in Eq. (2.7) (Dance *et al.*, 2014).

$$g(x, y) = \begin{cases} f(x, y) & T_1 \leq f(x, y) \leq T_2 \\ 0 & otherwise \end{cases} \tag{2.7}$$

Yussof and Burkhardt (2009) employed thresholding technique in liver segmentation. A 3D anisotropic diffusion was employed as pre-processing step to reduce noise while preserving the important details of the image. The image was segmented by thresholding method with threshold values that automatically selected from histogram of image. The input image and segmentation result are shown in Figure 2.10(a) and Figure 2.10(b) respectively. Then, 3D connected component was used to identify liver region and remove false liver region. The datasets used for evaluation were obtained from Hospital University of Freiburg. The percentage of volumetric overlap error was between 15% to 18%. The segmentation accuracy have to be improved for clinical application.

(a)   (b)
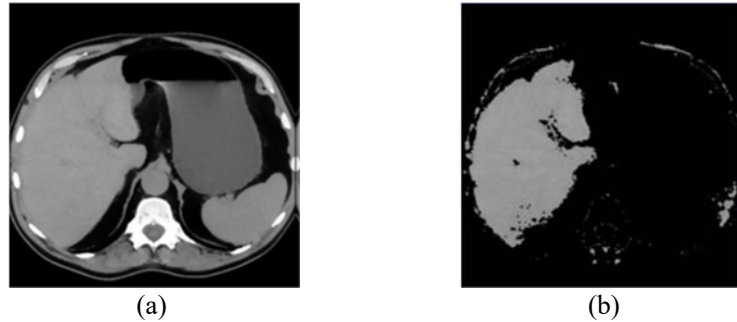
Figure 2.10: Thresholding technique. (a) Filtered image, (b) Result after thresholding (Yussof & Burkhardt, 2009)

Zayane *et al.* (2012) developed an automatic liver segmentation method by using thresholding technique. The interval for liver threshold was determined using histogram of CT image. The regions with intensity fall within interval of liver threshold were segmented. Median filter and morphological closing filter were applied to ameliorate image and fill the holes of regions. The largest connected component was identified using connected components labelling. Sobel filter was used to detect the contour of liver. The contour was used to segmented the liver region on the original image. The result was not satisfactory because the histogram varied with the input image. Peak representing liver in the histogram was different from dataset to dataset.

Irr and Rahni (2015) presented an automatic liver segmentation method by using low-level processing and shape model registration. Shape model was built using ground truth of data

sets using direct mesh to mesh registration. Multiple thresholding and distance transform were used in low-level processing stage to identify the range of intensity of dense tissue and locate the centre of liver. Then, the 3D binary image was used for shape model registration. The evaluation was done using data sets obtained from SLIVER07. Accuracy of segmentation was evaluated by using Jaccard index. The average Jaccard index of the evaluation of all images after shape registration was 0.64 ± 0.11 as compared to 0.39 ± 0.09 before shape registration. Liver boundaries need to be refined to improve the segmentation accuracy.

Thresholding technique is simple and time-efficient to extract liver parenchyma but does not produce satisfactory results in certain cases. Region of interest might be incorrectly labelled in noisy image because the intensity of pixel is out of the threshold interval due to the presence of noise. If liver region has low contrast with neighbouring organs, more advanced techniques need to be employed to improve the accuracy of segmentation (Dance *et al.*, 2014). The result may not be good if there are tumours present in the liver because the contrast between liver and tumour is significant (Luo *et al.*, 2014).

2.4.2 Region Growing

Region growing is a technique that merges pixels and sub-regions into larger regions based on criteria set. The region growing process starts with a set of "seed" points which are chosen based on user's criteria. The seed point as shown in Figure 2.11(a) grows by merging those neighbouring pixels that have predefined properties similar to the seed as shown in Figure 2.11(b). The growing process stops when region is expanded to the boundary of object (Gonzalez & Woods, 2006; Abd-Elaziz *et al.*, 2014).
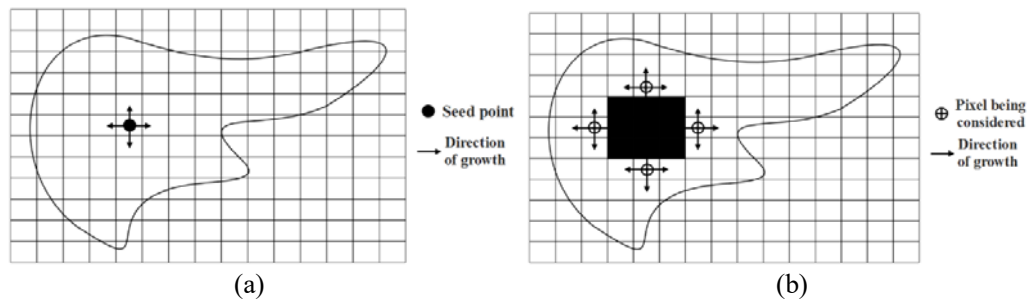
Figure 2.11: Region growing. (a) Start of region growing, (b) Growing process after a few iterations (Abd-Elaziz et al., 2014)

Wang and Gao (2012) developed a high-speed liver segmentation approach for abdominal CT image by employing mainly region growing method. The image was first remapped from 12-bit to 8-bit grey scale image. Then, the evanescent liver and discrete liver images were generated by thresholding method. The evanescent liver image was used as seed

points to remove non-liver region in the discrete liver image by region growing. Then, the discrete liver image was used to obtain minimum and maximum coordinates of discrete points for every rows and columns. The intensity of pixels within the range of minimum and maximum coordinates was recovered. Optimisation was done by edge correction removal of over-segmented region and 3D restoration. The dataset used were obtained from CT machine of hospital. The image format used was DICOM with 512×512 spatial resolution. The advantage of the approach was fast processing time. The disadvantage was the over-segmentation problem.

Lu *et al.* (2014) proposed an improved region growing algorithm for liver segmentation. In pre-processing stage, Gaussian filter was used for noise reduction. Next, to reduce the complexity of segmentation, thresholding was used to remove high grey level organs or tissues. Non-linear mapping was used to enhance the image contrast. Quasi-Monte Carlo method was used to select seed points for region growing. Then, region growing algorithm was applied for liver segmentation. In post-processing stage, Canny operator and flood-fill methods were used to fill out the holes and smooth the liver contour. The method was evaluated and the results showed 7.4% average volumetric overlap error, 4.6% relative volume difference, 1.2 mm average symmetric surface distance, 2.8 mm root mean square symmetric surface distance and 38.5 maximum symmetric surface distance. The results obtained was satisfactory for clinical application.

Arjun *et al.* (2015) presented an improved region growing method to improve the segmentation result of liver CT images. In pre-processing phase, Gaussian high boost filter was applied to reduce noise and sharpen the image followed by thresholding technique to remove high grey level organs and non-linear mapping to improve the image contrast. Then, segmentation process was done by using region growing method with seed points generated by Halton's quasi-random sequence. The region growing criteria was based on the average gradient of the seed points and grey scale average. The post-processing involved holes filling process. The datasets used were obtained from Cancer Imaging Archive. The method obtained good results with average accuracy of 0.9704, specificity of 0.9707, and sensitivity of 0.9690.

Problem arises in region growing approach if there are noise, sharp edges, and lines that formed disconnected boundaries because it is hard to formulate simple criteria to decide whether they are true region boundaries. Two regions could be joined to become single larger region if there is one small break in the boundary. Therefore, region growing method turns out to be a complex method because it requires gradually refining of the schemes to decide which pixels belong to which regions (Davies, 2012).

2.4.3 Active Contour

Active contour or snake is energy minimising spline influenced by external forces and internal forces. It is active because it always minimises the energy function dynamically. The internal forces impose piecewise smoothness constraint on the spline and push the contour to conform to nearby edges. The external forces serve to put the contour near the local minimum (Kass *et al.*, 1988). The internal energy consists of elastic energy and bending energy. The elastic energy is included to allow the snake to grow and shrink with penalty whereas the bending energy is included to restrict sharp corners and spikes in the snake. The external energy imposed constraints to the snake to prevent it from moving into prohibited region. The external energy allows the snake to interact with image features such as lines, edges, and termination. The snake energy function can be written as Eq. (2.8) (Davies, 2012).

$$
\begin{aligned}
E_{snake} &= E_{internal} + E_{external} \\
&= E_{internal} + (E_{image} + E_{constraints}) \\
&= E_{stretch} + E_{bend} + E_{line} + E_{edge} + E_{term} + E_{constraint}
\end{aligned}
\tag{2.8}
$$

where $E_{internal}$ is internal energy, $E_{external}$ is external energy, E_{image} is image energy, $E_{stretch}$ is elastic energy, E_{bend} is bending energy, E_{line} is line energy, E_{edge} is edge energy, E_{term} is termination energy, and $E_{constraint}$ is external constraint energy.

Xu and Prince (1998) introduced gradient vector flow (GVF) snake to overcome the problems arise due to the initialization process and poor convergence into boundary concavities. GVF snake was insensitive to initialization and capable of segmenting concave boundaries. Gradient vector flow fields were vector fields derived from energy minimization of image in a variational framework. GVF snake was differed from traditional snake because its external forces cannot be expressed as negative gradient of potential function. Figure 2.12 shows the application of a GVF snake in cardiac magnetic resonance image.
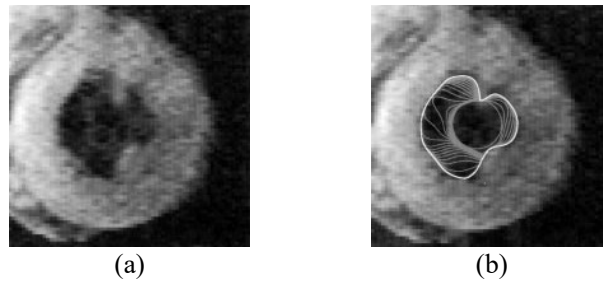

(a)   (b)

Figure 2.12: Cardiac MR segmentation using GVF snakes. (a) Original MRI image of left ventricle of human heart, (b) Convergence process of GVF snake (Xu & Prince, 1998)

Dawant *et al.* (2007) developed a semi-automatic liver segmentation method by using level-set approach and dynamically adapted speed function. A contour was drawn by user manually and one slice. Then, the level-set approach was used to drive the contour and stop at the boundaries. The average segmentation time required was about 20 minutes. The method was analysed using datasets provided by SLIVER07. The results showed average volumetric overlap error of 9.8%, relative volume difference of -6.2%, average symmetric surface distance of 1.6 mm, root mean square symmetric surface distance of 3.1 mm and maximum symmetric surface distance of 25 mm. The total score obtained was 63. The proposed method was unable to extract liver effectively when pathologies were present inside liver.

Suzuki *et al.* (2010) proposed a liver segmentation method by using geodesic active contour coupled with level-set contour evolution. Image was first undergone pre-processing to reduce noise and enhance anatomic structures. The anisotropic diffusion was used for noise reduction while scale-specific gradient magnitude filter was applied for boundary enhancement. Then, non-linear grey-scale converter was used in liver parenchyma contrast enhancement. The segmentation process involved two steps, fast-marching level-set algorithm was applied to generate initial rough contour of liver and geodesic active contour level-set algorithm was used to refine the liver boundary. The method achieved average accuracy of 98.4%, average sensitivity of 91.1%, average specificity of 99.1%, and average percent volume error of 7.2%. The inaccurate extraction was due to variable liver density and similar intensity of neighbouring organs with liver.

Goryawala *et al.* (2012) presented a 3-D liver segmentation technique by using modified *k*-means clustering with localised contour algorithm. The modified *k*-means clustering was used to produce five masks which are corresponding to five different regions. Optimal mask was produced by combining first two masks. The optimal mask was then used for contour initialization. Next, localised region based active contouring algorithm was used for liver segmentation. This approach was independent of dataset properties such as structure, size, position and intensity of liver.

The main advantage of active contour is it can capture the targeted object without a great definition of initial boundary (Luo *et al.*, 2014). Cremers *et al.* (2007) summarised several drawbacks of active contour approach. One drawback is there is possibility of snake self-interaction. Active contour does not allow topologies changes such as splitting or merging of the evolving contour. The snake might be biased or stuck in local minima as the algorithm is highly dependent on initialization. It is not straightforward to generalise snakes action to cover colour, texture, or motion because snakes lack of meaningful probabilistic interpretation.

2.4.4 Graph Cut

Graph cut is an approach that segment the graph into subgraph for each region. An undirected weighted graph is used to represent the image. The weight of edge represents the similarity between pair of adjacent pixels. The best cut can be achieved by making the similarity within a subgraph maximum while similarity between subgraphs minimum (Luo *et al.*, 2014). Boykov and Funka-Lea (2006) set the boundary penalties using Eq. (2.9).

$$B_{i,j} = \frac{1}{d_{i,j}} \, e^{-\frac{(I_i - I_j)^2}{2\sigma^2}} \tag{2.9}$$

where $B_{i,j}$ is penalty for a discontinuity between pixels i and j, $d_{i,j}$ is the distance between pixels i and j, I_i if the ith pixel intensity, I_j if the jth pixel intensity, and σ^2 can be estimated as Gaussian noise energy. $B_{i,j}$ is high for a pair of pixels of similar intensities, $|I_i - I_j| < \sigma$. $B_{i,j}$ is small if the pixels are very different, $|I_i - I_j| > \sigma$.

Beichel *et al.* (2012) developed a liver segmentation method using graph cuts with 3D segmentation refinement technique. The liver segmentation consisted of two phases, segmentation by graph cuts and interactive segmentation refinement. In first phase, thresholding was used to remove voxels with density below -600HU. Then, the effect non-liver structure on the gradient was reduced. Gaussian filter was applied to reduce noise and Gaussian gradient was computed for each voxel. Next, the weak edges were enhanced and surface measure was computed. Then, boundary cost term with weighting function was used to make costs of cut for all boundaries inexpensive. Graph cut algorithm was applied and was forced to follow the ridges of gradient, local non-maximal response. In refinement phase, thresholding was first used to generate binary volume. Then, the binary volume was logical OR with the graph cut image and the distance transform was computed. Next, watershed segmentation was applied and *H*-minima algorithm was employed to remove all small local minima due to quantization noise. Then neighbouring chunks with similar boundary voxels were merged together. After chunk-based refinement, mesh based refinement was applied by using deformable mesh model so that surface based refinement can be done in virtual reality user interface. The datasets of SLIVER07 were used to compare the developed method with other methods. The results showed 5.2% average volumetric overlap error, 1.0% relative volume difference, 0.8 mm average symmetric surface distance, 1.4 mm root mean square symmetric surface distance and 15.7 mm maximum symmetric surface distance. The method was able to give very good segmentation result and help user to save time up to 85%.

Peng *et al.* (2015) presented a semi-automatic 3D liver segmentation by employing multiple region appearance and graph cuts techniques. In pre-processing phase, linear interpolation was used to down sample the 3D CT image into $256 \times 256 \times 150 - 180$. Then, thresholding was used to remove the image outside the bounding box. In initialization phase, single-region appearance based model was initialized to optimise the energy so that the delineation of liver boundaries became more accurate. If the liver contained large tumours, multi-region appearance based model was used instead. In segmentation phase, graph cut technique with min cut max flow graph algorithm was applied for liver segmentation. The post-processing phase involved morphological closing operation and holes filling. The proposed method was analysed using datasets obtained from SLIVER07. The results showed average volumetric overlap error of $4.58\% \pm 0.51\%$, relative volume difference of $1.08\% \pm 0.80\%$, average symmetric surface distance of 0.68 ± 0.14 mm, root mean square symmetric surface distance of 1.45 ± 0.36 mm and maximum symmetric surface distance of 16.89 ± 3.69 mm. The method was able to delineate the surface of liver accurately and did not require user constraint on non-liver tissues and interactive refinement.

Li *et al.* (2015) proposed an automatic liver segmentation method by applying shape constraints and deformable graph cut. The CT images were smoothed by applying anisotropic diffusion filtering. Then, the mean liver shape was constructed and the position of liver was computed. Mesh was deformed and was adapted to the liver boundary. The deformable graph cut was used to detect the boundary accurately. The datasets used were obtained from SLIVER07 and 3D Image Reconstruction for Comparison of Algorithm Database (3DIRCADb). The results show average volumetric overlap error of $6.24\% \pm 1.52\%$, relative volume difference of $1.18\% \pm 2.76\%$, average symmetric surface distance of 1.03 ± 0.31 mm, root mean square symmetric surface distance of 2.11 ± 0.95 mm and maximum symmetric surface distance of 18.82 ± 8.82 mm. The method used was able to overcome the under-segmentation and over-segmentation. However, the accuracy has to be improved to deal with special anatomical structure of liver.

Graph cuts method is not automatic as it requires user to label the object and background. Hence, to make it fully automatic, algorithms have to be employed to select seed points. It is difficult to segment liver parenchyma because the seeds of background should include every other region. It is difficult to extract object from non-homogenous background too (Luo *et al.*, 2014).

2.4.5 Clustering Based Method

Clustering based method classifies pixels according to the similarity of pixels. Different tissues in CT or MRI have different image intensities. The simplest clustering method is *k*-means

clustering which classifies intensities of image into k clusters based on the image histogram. The *k*-means clustering minimises the variability of intensity within each cluster and is defined as Eq. (2.10) (Dance *et al.*, 2014).

$$\alpha_1^* \dots \alpha_N^* = \arg\min_{\{\alpha_1 \dots \alpha_N \in [1\dots k]\}} \sum_{j=1}^{k} \sum_{\{q:\alpha_q=j\}} (I_q - \mu_j)^2 \qquad (2.10)$$

where α_i is the cluster to which the pixel i is assigned, N is the number of pixels in an image, I_q is the intensity of pixel q, and μ_j is the mean of cluster j, i.e. mean intensity of all pixels assigned with label j. Other clustering methods includes fuzzy *c*-means clustering and Gaussian mixture modelling. In fuzzy *c*-means clustering, fuzzy set is used to describe partial cluster membership. In Gaussian mixture modelling, weighted sum of Gaussian probability densities is computed and fitted on the image histogram to find out the probability that a pixel belongs to a cluster (Dance *et al.*, 2014).

Li *et al.* (2013) presented an automatic liver segmentation of CT images by applying fuzzy *c*-mean clustering with level set. The segmentation process was divided into three stages, pre-processing, fuzzy *c*-mean clustering with level set segmentation and post-processing. In pre-processing stage, the histogram of image was analysed and the grey level range of liver was identified and extracted. Contrast enhancement was done on the image and median filter was applied to reduce noise and smooth the image. In the next stage, fuzzy c-mean clustering was adopted to locate the clusters containing liver and similar clusters were merged into larger clusters. The average intensity and standard deviation of each cluster were computed. Then, the clusters that did not belong to liver were rejected. Next, refinement of segmentation was done using distance regularised level set. The last stage was post-processing which involved morphological opening operation, largest region selection, median filtering and hole-filling. The experiment showed accuracy of 0.9986 and specificity of 0.9989. The method can give good segmentation result even though the boundary was not clear but the under-segmentation problem still existed when there were vessels or homogeneous tissues near the edge of liver.

Foruzan *et al.* (2013) proposed a liver segmentation approach by adopting *k*-means clustering, narrow band thresholding and geodesic active contour algorithm. In pre-processing stage, border of liver was defined by doctor. Then, the abdominal region was extracted using thresholding method. Then, the bounding box of abdominal was identified. Next, thresholding technique was applied again to remove ribs. Dynamic Gaussian mixture model was used to represent the intensity distribution of liver. The parameter of the model was estimated using expectation maximisation algorithm. Narrow band thresholding was used to locate candidate

pixels. The *k*-means clustering was employed to determine whether a candidate pixel was within liver region or not. The anisotropic diffusion filtering was employed to smooth the image. Then, the image was converted to binary image. The non-liver regions were removed by directed graph search method. After that, the liver boundary was smoothed by using Fourier transform. Finally, geodesic active contour algorithm was employed to find the final liver surface. The approach was evaluated using datasets from Shiga University of Medical Science, Osaka University Hospital and SLIVER07. The results of SLIVER07 dataset showed average volumetric overlap error of 8.29%, relative volume difference of 1.75%, average symmetric surface distance of 1.38 mm, root mean square symmetric surface distance of 2.73 mm and maximum symmetric surface distance of 27.16 mm. The method performed well in low contrast images.

The advantage of clustering-based methods is they are fully automatic. Nevertheless, the segmentation result may contain false-positive regions which require post-processing. *k*-means clustering usually does not use as main segmentation method because it is too rough. *k*-means clustering is often used to select object and background seeds for graph cuts, and initial boundary of active contour (Luo *et al.*, 2014).

2.4.6 Morphological Operations

Mathematical morphology is a tool for extracting image components that are useful in the representation and description of region shapes, such as boundaries, skeletons, and convex hulls. Mathematical morphology can be applied on binary images and grey-scale images. The two types of basic morphological operations are dilation and erosion. Erosion shrinks or thins objects in a binary image. Hence, erosion can be viewed as morphological filtering operation in which the image details smaller than the structuring element are filtered out. Erosion of A by B, denoted $A \ominus B$ is defined as Eq (2.11) (Gonzalez & Woods, 2006). Unlike erosion, which is a shrinking or thinning operation, dilation grows or thickens objects in binary image. Dilation of A by B, denoted $A \oplus B$ is defined as Eq. (2.12) (Gonzalez & Woods, 2006).

$$A \ominus B = \{z | (B)_z \subseteq A\} \tag{2.11}$$

$$A \oplus B = \left\{z | (\hat{B})_z \cap A \neq \emptyset\right\} \tag{2.12}$$

where A is input image, B is structuring element, $(B)_z$ is the translation of B by the vector z, $\emptyset$ is empty set, $\hat{B}$ is reflection of structuring element about its origin, $(\hat{B})_z$ is the translation of $\hat{B}$ by vector z.

Another two important morphological operations are opening and closing. Morphological opening is used to smooth the contour, break narrow isthmuses, and eliminate thin protrusions. Morphological opening of input image A by structuring element B, denoted by $A \circ B$, is defined as Eq. (2.13) (Gonzalez & Woods, 2006). Morphological closing is used to smooth sections of contours but, as opposed to opening, it is used to fuse narrow breaks, eliminate small holes, and fill gaps in the contour. Morphological closing of image A by structuring element B, denoted by $A \bullet B$ is defined as Eq. (2.14) (Gonzalez & Woods, 2006).

$$A \circ B = (A \ominus B) \oplus B \qquad (2.13)$$

$$A \bullet B = (A \oplus B) \ominus B \qquad (2.14)$$

where A is input image, B is structuring element, $\ominus$ is erosion operator and $\oplus$ is dilation operator.

Hole-filling or region-filling is another type of morphological algorithm that often used in pre- or post-processing steps. Hole is defined as a background region surrounded by a connected border of foreground pixels. Hole-filling algorithm is based on dilation, complementation and intersection. The hole-filling process begins with a point, X_0 inside a hole as shown in Figure 2.13, the hole-filling is done using Eq. (2.15) (Gonzalez & Woods, 2006).

$$X_k = (X_{k-1} \oplus B) \cap A^c \qquad k = 1, 2, 3, \ldots \qquad (2.15)$$

where X_k is set containing filled holes, k is number of iteration, B is the structuring element, $\oplus$ is dilation operator, $\cap$ is the intersection operator, A^c is the complement of set A. The algorithm terminates at iteration step $X_k = X_{k-1}$. The dilation of hole-filling is conditional so that Eq. (2.15) would not fill the entire area. The output of hole-filling process is the set union of X_k and A contains the filled hole and its boundary (Gonzalez & Woods, 2006).

The process of hole-filling is illustrated in Figure 2.13. The object pixels are represented by white colour whereas the background pixels are represented by grey colour in Figure 2.13. Given input of set A as shown in Figure 2.13(a), the complement of set A, A^c as shown in Figure 2.13(b) is obtained. The structuring element B used in the hole-filling process is as shown in Figure 2.13(c). The hole-filling process is started by selecting a point in the hole as shown in Figure 2.13(d). Then, Eq. (2.15) is applied for subsequent iterations if there is an object pixel in its 4-connected neighbourhood. The results of first and second iteration are shown in Figure 2.13(e) and Figure 2.13(f) respectively. After seven iterations, the algorithm is terminated as the hole within the boundary is filled. The result of seventh iteration is shown in Figure 2.13(g). The